Differentiating surface and bulk interactions using localized surface plasmon resonances of gold nanorods

Neha Nehru,[1] Eugenii U. Donev,[1,3] Gazi M. Huda,[1] Linliang Yu,[2] Yinan Wei,[2] and J. Todd Hastings[1,*]

[1]*Electrical and Computer Engineering, University of Kentucky, Lexington, Kentucky 40506, USA*
[2]*Department of Chemistry, University of Kentucky, Lexington, Kentucky 40506, USA*
[3]*Currently with Brookhaven National Laboratory, Upton, NY 11973, USA*
**hastings@engr.uky.edu*

Abstract: We demonstrate a novel localized surface-plasmon resonance sensor that can distinguish surface binding interactions from interfering bulk effects. This is accomplished by utilizing the longitudinal and transverse plasmon modes of gold nanorods. We have investigated, both numerically and experimentally, the effect of change in background refractive index and surface binding on the two resonances of a gold nanorod on an indium tin oxide coated glass substrate.

OCIS codes: (250.5403) Plasmonics; (280.4788) Optical sensing and sensors.

References and links

1. K. A. Willets and R. P. Van Duyne, "Localized surface plasmon resonance spectroscopy and sensing," Annu. Rev. Phys. Chem. **58**(1), 267–297 (2007).
2. S. A. Maier and H. A. Atwater, "Plasmonics: localization and guiding of electromagnetic energy in metal/dielectric structures," J. Appl. Phys. **98**(1), 011101 (2005).
3. J. J. Mock, M. Barbic, D. R. Smith, D. A. Schultz, and S. Schultz, "Shape effects in plasmon resonance of individual colloidal silver nanoparticles," J. Chem. Phys. **116**(15), 6755–6759 (2002).
4. E. Stefan Kooij and B. Poelsema, "Shape and size effects in the optical properties of metallic nanorods," Phys. Chem. Chem. Phys. **8**(28), 3349–3357 (2006).
5. A. J. Haes and R. P. Van Duyne, "A unified view of propagating and localized surface plasmon resonance biosensors," Anal. Bioanal. Chem. **379**(7-8), 920–930 (2004).
6. J. Homola, "Surface plasmon resonance sensors for detection of chemical and biological species," Chem. Rev. **108**(2), 462–493 (2008).
7. C. J. Murphy, T. K. Sau, A. M. Gole, C. J. Orendorff, J. Gao, L. Gou, S. E. Hunyadi, and T. Li, "Anisotropic metal nanoparticles: Synthesis, assembly, and optical applications," J. Phys. Chem. B **109**(29), 13857–13870 (2005).
8. A. J. Haes, S. Zou, G. C. Schatz, and R. P. Van Duyne, "A nanoscale optical biosensor: the long range distance dependence of the localized surface plasmon resonance of noble metal nanoparticles," J. Phys. Chem. B **108**(1), 109–116 (2004).
9. M. Pelton, J. Aizpurua, and G. Bryant, "Metal-nanoparticle plasmonics," Laser Photonics Rev. **2**(3), 136–159 (2008).
10. J. Homola, "Present and future of surface plasmon resonance biosensors," Anal. Bioanal. Chem. **377**(3), 528–539 (2003).
11. J. T. Hastings, J. Guo, P. D. Keathley, P. B. Kumaresh, Y. Wei, S. Law, and L. G. Bachas, "Optimal self-referenced sensing using long- and short- range surface plasmons," Opt. Express **15**(26), 17661–17672 (2007).
12. J. Homola, H. B. Lu, and S. S. Yee, "Dual-channel surface plasmon resonance sensor with spectral discrimination of sensing channels using dielectric overlayer," Electron. Lett. **35**(13), 1105–1106 (1999).
13. R. Slavík, J. Homola, and H. Vaisocherová, "Advanced biosensing using simultaneous excitation of short and long range surface plasmons," Meas. Sci. Technol. **17**(4), 932–938 (2006).
14. J. Guo, P. D. Keathley, and J. T. Hastings, "Dual-mode surface-plasmon-resonance sensors using angular interrogation," Opt. Lett. **33**(5), 512–514 (2008).
15. V. Sharma, K. Park, and M. Srinivasarao, "Colloidal dispersion of gold nanorods: Historical background, optical properties, seed-mediated synthesis, shape separation and self-assembly," Mater. Sci. Eng. Rep. **65**(1-3), 1–38 (2009).
16. C. Bohren and D. Huffman, *Absorption and Scattering of Light by Small Particles* (Wiley, 1998).

#160115 - $15.00 USD Received 15 Dec 2011; revised 7 Mar 2012; accepted 10 Mar 2012; published 12 Mar 2012

17. P. B. Johnson and R. W. Christy, "Optical constants of the noble metals," Phys. Rev. B **6**(12), 4370–4379 (1972).
18. G. M. Huda, E. U. Donev, M. P. Mengüç, and J. T. Hastings, "Effects of a silicon probe on gold nanoparticles on glass under evanescent illumination," Opt. Express **19**(13), 12679–12687 (2011).
19. X. Huang, S. Neretina, and M. A. El-Sayed, "Gold nanorods: from synthesis and properties to biological and biomedical applications," Adv. Mater. (Deerfield Beach Fla.) **21**(48), 4880–4910 (2009).
20. K. M. Mayer, S. Lee, H. Liao, B. C. Rostro, A. Fuentes, P. T. Scully, C. L. Nehl, and J. H. Hafner, "A label-free immunoassay based upon localized surface plasmon resonance of gold nanorods," ACS Nano **2**(4), 687–692 (2008).
21. H. Chen, X. Kou, Z. Yang, W. Ni, and J. Wang, "Shape- and size-dependent refractive index sensitivity of gold nanoparticles," Langmuir **24**(10), 5233–5237 (2008).

1. Introduction

Metal nanoparticles supporting localized surface plasmon resonances (LSPR) have been extensively studied as label free sensors in various biological, chemical, environmental and medical applications [1]. LSPR is the result of the collective oscillation of conduction electrons in a metal nanostructure when illuminated with light. Excitation of surface plasmon resonances leads to enhanced absorption and scattering of the incident light along with strong localization of electromagnetic fields around the metal surface at the resonant frequency [2]. This plasmon resonance depends on the particle size, shape, material as well as the optical properties of the surrounding medium [3–5].

The fundamental sensing mechanism of LSPR sensors is similar to that of propagating surface plasmon resonance (SPR) sensors. Such sensors detect target molecules by measuring the change in the refractive index that occurs near the surface when the analyte binds to the functionalized metal nanostructure. This change in the refractive index is directly measured from the shift in the resonance wavelength in the absorption or scattering spectrum [5,6]. Advantages of LSPR sensors over the traditional propagating SPR sensors include greater field enhancement at the metal surface, significantly reduced sensing volumes and extensive resonance wavelength tenability [7–9]. Despite their advantages, LSPR sensors suffer from the same limitations as propagating SPR sensors. In particular, these sensors cannot distinguish specific target interactions from various non-specific interfering effects. These effects include variations in the solution refractive index and non-specific binding between the sensor and non-target molecules [10].

These interactions can severely compromise the measurement of the target analyte in a complex unknown media and hence limit the applicability and impact of LSPR sensors. Various groups have investigated the use of multiple surface plasmon waves in a thin film SPR sensor to differentiate between surface and bulk effects [11–14]. However, there has been a notable absence of efforts to make LSPR sensors more immune to interfering effects. To address this problem we have investigated a self-referencing technique that utilizes the multiple plasmon modes of a metallic nanostructure to distinguish target analyte from non-specific interactions. For example, to differentiate solution refractive index changes from surface binding interactions we would require a nanostructure that supports at least two surface plasmon resonances. Ellipsoidal or rod-like particles are some of the simplest structures that exhibit dual plasmon resonances, longitudinal and transverse, depending on whether the incident electric field is polarized along the long axis or the short axis of the particle [15]. The longitudinal plasmon resonance wavelength of such structures depends on the length of the nanorod and can be tuned anywhere from visible to near-IR [4].

If we assume that the two resonance wavelengths of the nanoparticle are linearly related to changes in the solution refractive index and to the surface coverage of bound analyte, then the change in the longitudinal and transverse surface plasmon resonance can be expressed as

$$\Delta\lambda_L = S_{BL}\Delta n_B + S_{SL}\Delta C_S \quad (1)$$

$$\Delta\lambda_T = S_{BT}\Delta n_B + S_{ST}\Delta C_S \quad (2)$$

#160115 - $15.00 USD Received 15 Dec 2011; revised 7 Mar 2012; accepted 10 Mar 2012; published 12 Mar 2012

where S_{BL} and S_{BT} are the bulk refractive index sensitivities and S_{SL} and S_{ST} are the surface binding sensitivities of the longitudinal and transverse plasmon modes respectively. Δn_B is the bulk refractive index change and ΔC_s represent the surface coverage of the adsorbed layer. If the bulk and surface sensitivities and resonance wavelength shifts are known, the surface coverage and bulk index changes can be calculated directly from

$$\Delta C_S = \frac{\frac{\Delta\lambda_T}{S_{BT}} - \frac{\Delta\lambda_L}{S_{BL}}}{\frac{S_{ST}}{S_{BT}} - \frac{S_{SL}}{S_{BL}}} \tag{3}$$

$$\Delta n_B = \frac{\frac{\Delta\lambda_T}{S_{ST}} - \frac{\Delta\lambda_L}{S_{SL}}}{\frac{S_{BT}}{S_{ST}} - \frac{S_{BL}}{S_{SL}}} \tag{4}$$

Simple calculations using the electrostatic approximation for a core shell ellipsoidal structure in a homogenous medium [16] suggest that the longitudinal and transverse resonances of a nanorod respond differently to surface and bulk interactions and can be used to differentiate these effects.

2. Simulation

To further test this theory, numerical simulations were carried out to study the effect of bulk and surface changes on a gold nanorod supported on a substrate. We used a commercially available finite element method package (COMSOL 3.5a, RF module) for all simulations. A spherical simulation domain was used to model the scattering from a gold nanorod on a 60-nm thick indium-tin-oxide (ITO) layer with an underlying glass substrate as shown in Fig. 1(a). As discussed later, the ITO coating was used to simplify the electron-beam lithography process. The simulation domain was subdivided into two halves to represent the substrate and the surrounding medium. The nanorod was modeled as a two dimensional elliptic cylinder with maximum lateral dimensions of 133 nm by 73 nm extruded to a height of 30 nm into the spherical simulation domain. The substrate was defined using a constant refractive index for glass (n = 1.5) and ITO (n = 2.0). Optical constants for gold were obtained from Johnson and Christy [17]. The simulations were conducted by defining the source field throughout the volume of the simulation domain as if the nanorod were absent. Then the scattered field was calculated with the nanorod present [18]. All simulations were validated against Mie theory and by confirming that the scattered field is approximately zero in the absence of a nanorod (more detail about the simulation and validation techniques can be found in [18]).

To calculate the bulk sensitivity of the nanorod, the refractive index of the medium was increased by 0.068 refractive index units (RIU). To calculate the surface sensitivity, a uniform thin shell (n = 1.45, thickness = 5 nm) was added to the gold nanorod to represent the presence of a bound analyte over the entire surface. The entire simulation space was surrounded by a perfectly matched layer (PML) tailored to the medium refractive index. The source field was defined analytically as a plane wave incident at an angle of 37.52° from within the substrate (the average angle of illumination from the darkfield objective used in our experiments). The scattering spectrum was obtained by integrating the Poynting vector for the scattered field over the boundary of the glass substrate defined by a numerical aperture (NA) of 0.5.

Figure 1(b) shows the calculated scattering spectra obtained from the nanorod sensor with bulk refractive index or surface coverage changes. The longitudinal and transverse resonances shift by different amounts with surface and bulk interactions and thus can help differentiate the two effects. Table 1 shows the bulk and surface sensitivities (assuming complete surface coverage) for the two modes calculated using the above model. A figure of merit (χ) for a

#160115 - $15.00 USD Received 15 Dec 2011; revised 7 Mar 2012; accepted 10 Mar 2012; published 12 Mar 2012

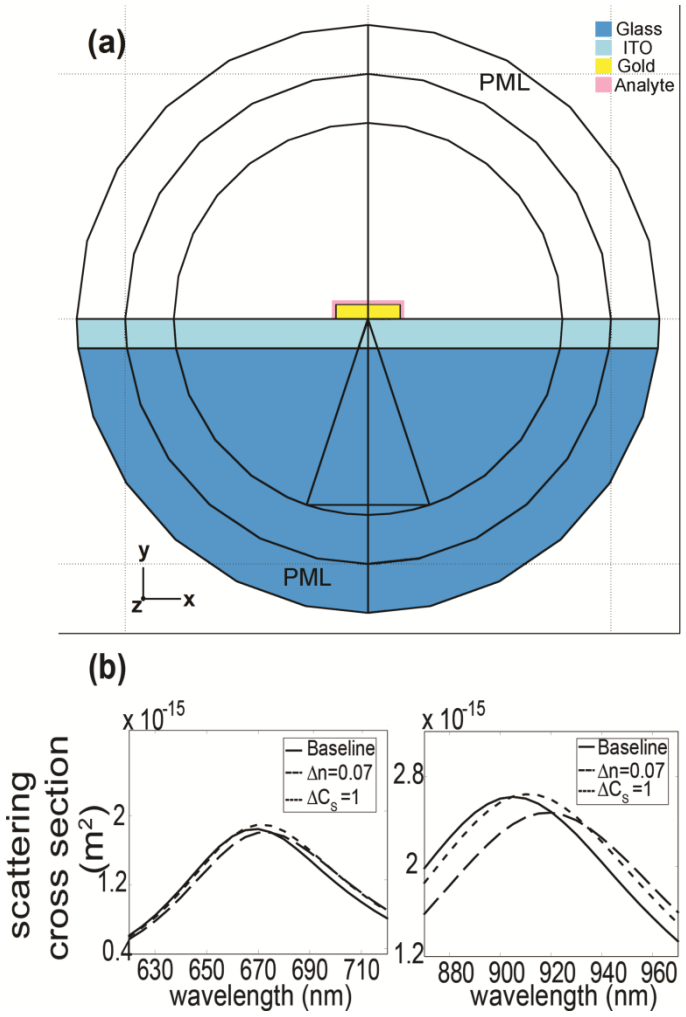

Fig. 1. (a) Cross section of the geometry used for simulation measurements, and (b) Calculated transverse (left) and longitudinal (right) resonance for a gold nanorod on ITO coated glass substrate. The shift in resonance wavelengths is due to either a change in solution index by 0.068 RIU or adsorption of a 5-nm thick layer.

dual mode sensor is proportional to the difference between the ratios of bulk and surface sensitivities, where $\chi \equiv \left| S_{BL}/S_{BT} - S_{SL}/S_{ST} \right|$ [13]. A larger figure of merit indicates lower cross-sensitivity, and better differentiation between the two effects. The bulk and surface sensitivity ratios and figure of merit for our nanorod based dual mode sensor were calculated to be 3.7, 2.6 and 1.0 respectively. The figure of merit is smaller than that of a traditional dual mode propagating SPR sensor (χ = 1.4) [11]. However, detection occurs in a dramatically smaller volume using LSPR.

Table 1. Calculated bulk and surface sensitivities for the longitudinal and transverse surface plasmon modes

	Bulk sensitivity (nm/RIU)	Surface sensitivity (nm for complete coverage)
Transverse mode	54	2.2
Longitudinal mode	200	5.8

#160115 - $15.00 USD Received 15 Dec 2011; revised 7 Mar 2012; accepted 10 Mar 2012; published 12 Mar 2012

3. Biosensing experiment

In order to ascertain the self-referencing performance of a dual mode sensor we performed the well characterized biotin-streptavidin binding experiment on an array of gold nanorods. The nanorods were fabricated using electron beam lithography (Raith E-LiNE) on an indium tin oxide (ITO) coated glass substrate (SPI Supplies) spin coated with polymethyl methacrylate (PMMA). The indium tin oxide coating mitigated charging during lithographic exposure and also improved adhesion of the gold compared to uncoated BK7 glass substrates. As a result, no additional adhesion layer, such as Ti or Cr, was required. Gold nanorod arrays were formed by sputtering a 30-nm thick gold film on the patterned surface followed by lift off in N-methyl pyrrolidone (NMP). Scanning electron micrograph (SEM) images of nanorod arrays of different dimensions are shown in Fig. 2.

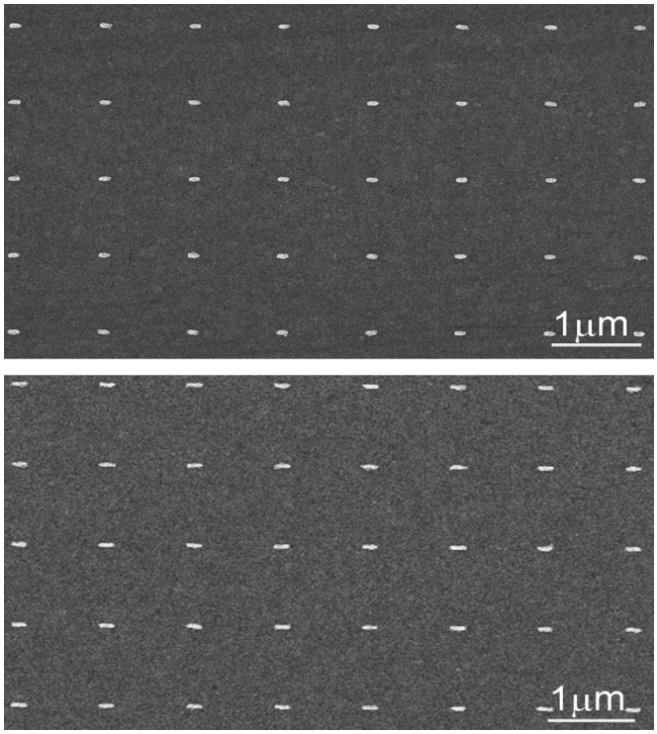

Fig. 2. SEM images of nanorod arrays of sizes 125nm by 57nm (top) and 182nm by 69nm (bottom) and a pitch size of 1μm fabricated using electron beam lithography.

Figure 3 illustrates the experimental setup used for scattering measurements. The apparatus was built around a Zeiss Axiovert 405M inverted microscope. Light from a 100W halogen lamp was incident on the sensor surface through a 20X dark field objective (NA = 0.5). Scattered light collected using the same objective was routed through an adjustable aperture and a Glan-Taylor polarizer (Thorlabs Inc.) to a grating spectrograph (Acton SP-150) and thermoelectric cooled CCD camera (Princeton Instruments PIXIS 256). All spectra were normalized to the scattering from the bare substrate.

Figures 4(a) and 4(b) show the normalized transverse and longitudinal scattering spectra of the 110nm by 54nm nanorod array in air and water. Both the modes exhibit a strong dependence to the surrounding medium, red shifting with increasing refractive index. Scattered light was collected from an area containing approximately 80 nanorods. Figure 4(c) displays the unpolarized scattering spectra of nanorod arrays of various sizes. The longitudinal mode strongly depends on the size of the nanorod, red shifting with increasing nanorod length, while the transverse mode shows a slight increase in the scattering intensity [19].

#160115 - $15.00 USD Received 15 Dec 2011; revised 7 Mar 2012; accepted 10 Mar 2012; published 12 Mar 2012

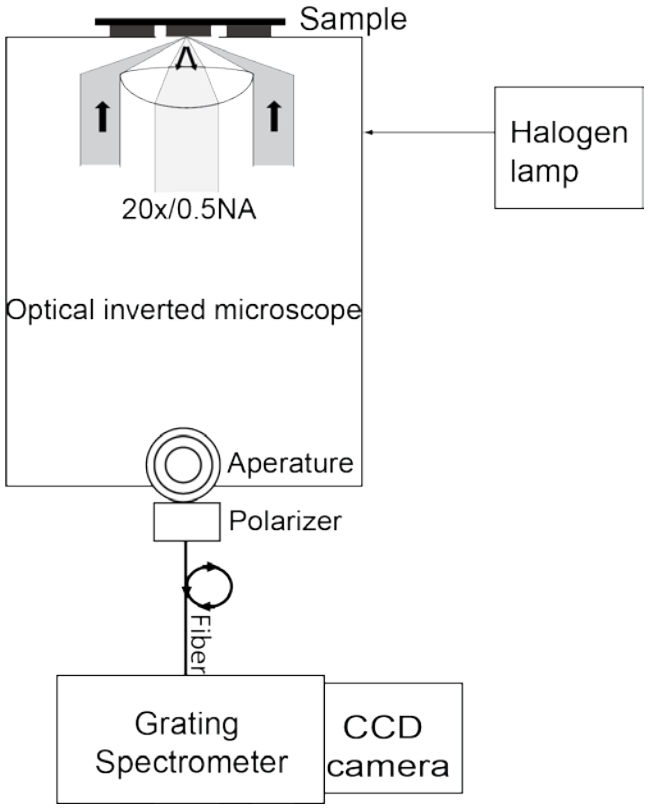

Fig. 3. Schematic of the optical setup used for scattering measurements.

After characterization, sample containing gold nanorod arrays with an approximate dimension of 130nm by 70nm was incubated overnight in a 10 mM phosphate buffer solution (pH 7.2) containing 200 μM of N-(6-[biotinamido]hexyl)-3′-(2’-pyridyldithio)propionamide (Biotin-HPDP, Pierce Biotechnology) at room temperature for biotin labeling. The coated surface was rinsed with deionized water and air-dried. The sensor was clamped in a custom made acrylic flow cell with fluorinated ethylene propylene (FEP) coated channels. It was then placed on the microscope stage and the unpolarized scattering measurements were recorded using custom software developed in LabView (National Instruments) that separately tracked the longitudinal and transverse resonances in each spectrum. Solutions were introduced to the sensor surface through polytetrafluoroethylene (PTFE) tubing at a constant flow rate of 500 μl/min using a low pulsation peristaltic pump (Ismatec). A 50 mM Tris buffer (pH = 8.0) solution was used as the baseline to carry out the sensing experiments. The buffer solution was modified by adding either glycerol (Fisher Scientific) to a final concentration of 50% (w/v) to change the background refractive index by $\Delta n_B = 0.068$ or streptavidin to a final concentration of 0.2 mg/ml (Pierce Biotechnology) to provide a surface binding interaction.

Figures 5(a) and 5(b) display the response of the longitudinal and transverse modes of the nanorod sensor to bulk solution change and streptavidin binding. Figures 5(c) and 5(d) show the bulk refractive index change and change in fractional surface coverage as functions of time calculated using the model described in Eqs. (3) and (4). There is a small amount of crosstalk between the two modes that leads to a small bulk index error for times greater than 2500 s, as shown in Fig. 5(c). This can likely be attributed to the calibration errors, small baseline drift, or nonlinearity in the sensor response. More interestingly, there are dynamic effects which lead to large spikes in the surface coverage estimates during solution index

#160115 - $15.00 USD Received 15 Dec 2011; revised 7 Mar 2012; accepted 10 Mar 2012; published 12 Mar 2012

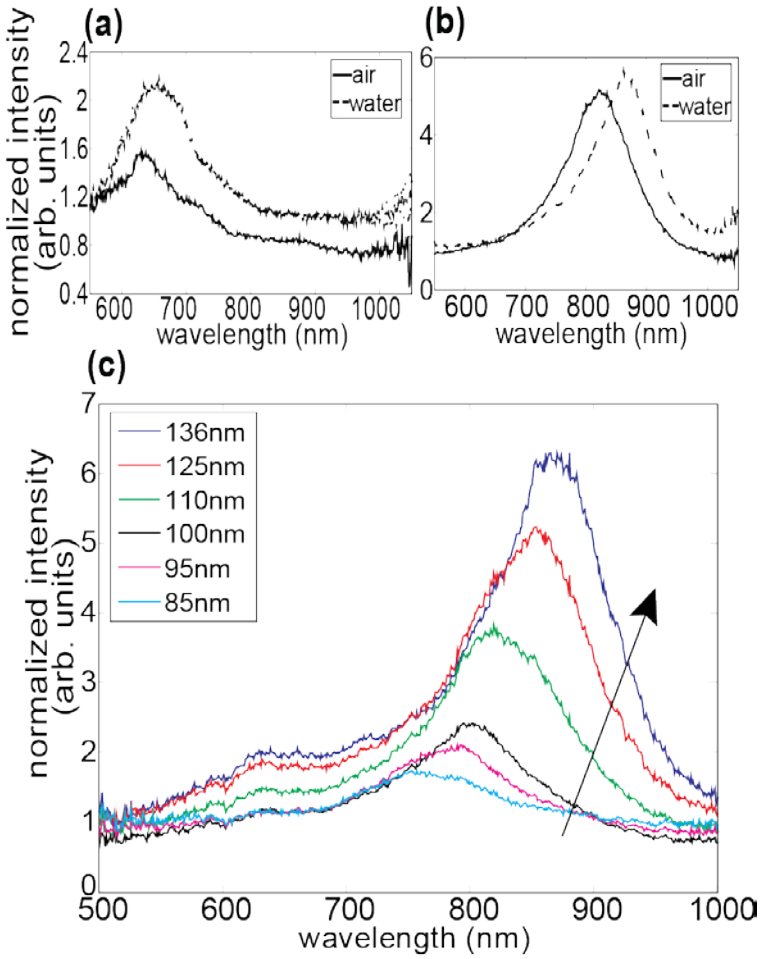

Fig. 4. Shift in (a) transverse and (b) longitudinal resonance for an array of nanorods of size 110nm by 54nm with a change in surrounding refractive index from air to water and,(c) unpolarized scattering spectra for nanorod arrays of various sizes. Arrow indicates increasing rod length as indicated in the legend. The width of these nanorods range from 50 to 58nm.

changes as can be seen in Fig. 5(d), when the solution is switched from pure buffer to buffer with glycerol. These dynamic effects were also observed with a similar gold nanorod array sensor (Fig. 6(d)). It should be noted that in both sets of data, this effect is only present when there is an abrupt shift in the resonance wavelengths as witnessed in Figs. 5(a) and 5(b) when the solution is changed from buffer to buffer with glycerol. No such effect is observed when the resonance wavelengths shifts gradually which occurs during the introduction of streptavidin with buffer solution. From a practical standpoint, these dynamic errors may or may not be acceptable depending upon the rate of change of the bulk index.

The bulk sensitivities for the longitudinal and transverse modes of the nanorod sensor were calculated using the linear model [Eqs. (1) and (2)] and found to be 145 nm/RIU and 55nm/RIU respectively. Although it is difficult to quantify the surface concentration of streptavidin, we can evaluate the ratio of the surface sensitivities for the longitudinal and transverse mode. The ratios of bulk and surface sensitivities and the figure of merit for our nanorod sensor were calculated to be S_{BL}/S_{BT} = 2.6, S_{SL}/S_{ST} = 3.5 and χ = 0.88. These results are within 35% of the sensitivities and figure of merit values obtained from simulation model. The minor difference between the two can likely be attributed to various experimental details

#160115 - $15.00 USD Received 15 Dec 2011; revised 7 Mar 2012; accepted 10 Mar 2012; published 12 Mar 2012

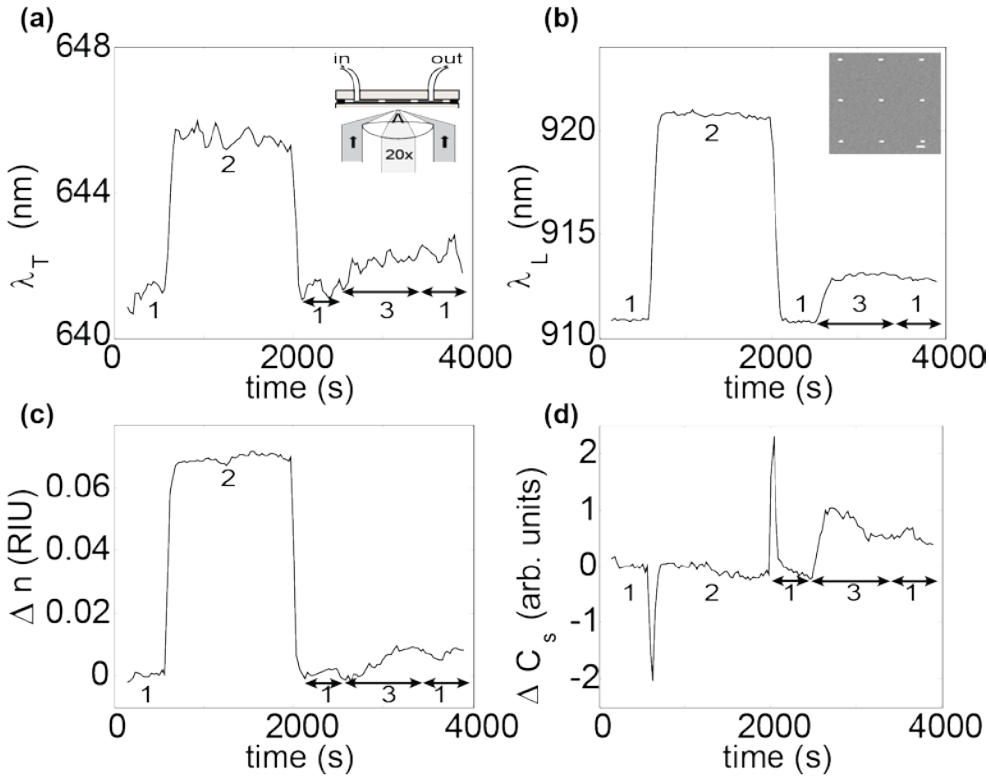

Fig. 5. Sensor response of biotin functionalized gold nanorod array to streptavidin binding. (a,b) Shift in transverse and longitudinal resonance wavelength versus time. (c,d) Bulk refractive index and relative surface layer coverage calculated from (a,b). The solutions were introduced through the flowcell in the following order: (1) buffer, (2) buffer with 50% glycerol, and (3) buffer with streptavidin. Inset in (a) shows a schematic of the flow cell and (b) SEM image of the nanorods used for sensing. Scale bar represents 200nm.

not accounted for in the simulation, including the surface roughness and optical absorption of the ITO coating on the glass substrate, the non-ellipsoidal cross-section and vertically tapered sidewalls of the gold nanorod, and possibly non-uniform coating of the biotin and streptavidin layers on the surface of the sensor.

To further validate the response of gold nanorods to bulk and surface interactions we conducted the same sensing experiment on similar sized nanorod array also fabricated using electron beam lithography. Figures 6(a) and 6(b) show the change in the transverse and longitudinal resonance wavelength while Figs. 6(c) and 6(d) show the calculated bulk refractive index and surface changes. As expected, we see large spikes in Fig. 6(d) when the solution is changed from buffer to buffer with glycerol. The bulk sensitivities calculated using the linear model for this sensor are 240 nm/RIU and 150 nm/RIU for longitudinal and transverse resonance modes respectively. The ratio of bulk and surface sensitivities along with the figure of merit was found to be 1.6, 1.3 and 0.25 respectively. The disparity in the sensitivities and figure of merit values measured for the two nanorod arrays could be the result of different end shape geometries as the second array, shown inset in Fig. 6(b), exhibited a more rectangular shape and poorer quality liftoff.

The surface limit of detection (LOD) at three standard deviations for the better nanorod array sensor, in terms of fractional surface coverage of streptavidin, was calculated to be 0.1595. This value is considerably higher than that of a traditional dual mode SPR sensor [11], but the sensing volume is dramatically smaller. The ratio of sensitivity to the full width at half-maximum (FWHM) of the resonance, which is a common figure of merit for single mode

#160115 - $15.00 USD Received 15 Dec 2011; revised 7 Mar 2012; accepted 10 Mar 2012; published 12 Mar 2012

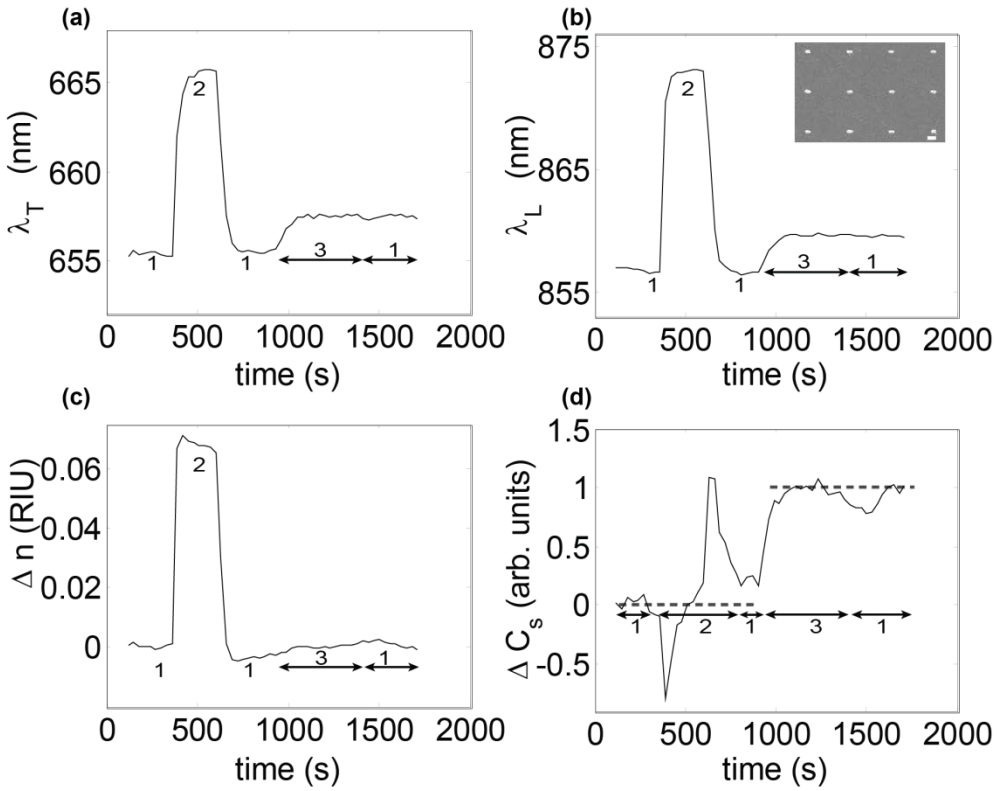

Fig. 6. Sensor response of biotin functionalized gold nanorod array to streptavidin binding. (a,b) Shift in transverse and longitudinal resonance wavelength versus time. (c,d) Bulk refractive index and relative surface layer coverage calculated from (a,b). The solutions were introduced through the flowcell in the following order: (1) buffer, (2) buffer with 50% glycerol, and (3) buffer with streptavidin. Inset in (b) displays the SEM image of the nanorod used for sensing. Scale bar is 200nm.

sensors and is indirectly related to LOD, was determined to be 1.9. The longitudinal mode bulk sensitivity for our sensor is somewhat lower than those measured by Mayer et al. [20] and Chen et al. [21] for chemically synthesized gold nanorods. On the other hand, our ratio of sensitivity to full width at half-max is higher than the value reported by Mayer et al. [20]. In each case the aspect ratio of the rods varied from ours, a factor which can significantly impact the sensitivity. It should be noted that the structures used in these experiments have not yet been optimized to obtain the lowest limits of detection, but still clearly demonstrate that a nanorod array based sensor can differentiate surface interactions from bulk index changes.

4. Conclusions

We have shown through both simulations and experiments that the two localized surface-plasmon resonances of a gold nanorod can compensate for changes in the background refractive index and allow surface binding of the target analyte to be measured separately. These sensors exhibit comparable performance to other nanorod LSPR sensors with the added benefit of bulk index compensation. When compared to traditional SPR sensors based on propagating surface plasmons, these sensors offer dramatically reduced sensing volume, but will require further optimization to achieve similar figures of merit and limits of detection.

#160115 - $15.00 USD Received 15 Dec 2011; revised 7 Mar 2012; accepted 10 Mar 2012; published 12 Mar 2012

Acknowledgments

This material is based upon work supported by the National Science Foundation under Grant No. ECCS-0747810. Facilities and technical assistance for this work were provided by the University of Kentucky Center for Nanoscale Science and Engineering (CeNSE) which received support under NSF award No. EPS-0447479

#160115 - $15.00 USD Received 15 Dec 2011; revised 7 Mar 2012; accepted 10 Mar 2012; published 12 Mar 2012